



A device for rapid calorimetric measurements on small biological tissue samples

Johannes Lerchner¹ · Livia S. Hervas² · Kenia C. Bícigo² · Geovana S. Garcia³ · Marcos T. Oliveira³ · Mersiha Hasic^{4,5} · Martin Klingenspor^{4,5} · Florian Mertens¹

Received: 29 December 2023 / Accepted: 4 April 2024
© The Author(s) 2024

Abstract

A new calorimetric technique is described that allows high-throughput heat production rate measurements on small biological tissue samples. The technique is based on the widely used thermopile chip technology combined with an innovative method for precise transport and positioning of samples of different biological materials at the thermal power detector inside the calorimeter. The new transport and positioning technique is a combination of fluidic and mechanical transport, where the latter is realized by a magneto-motor drive. The transport facility ensures good diffusive oxygen penetration into the sample, which is essential for highly metabolically active materials. The proper functioning of the device is demonstrated by measuring the heat production of metabolically active brown adipose tissue, biopsied tegu lizard muscle, and live *Drosophila* larvae at different stages and temperatures.

Keywords Chip calorimetry · Biological tissues · Brown adipose tissue · *Drosophila* larvae · Tegú lizard muscle tissue

Introduction

The driving force of metabolic processes within a biological entity is determined by its internal entropy production, which is released to the environment as heat. Entropy production is the result of the chemical work associated with the numerous biochemical reactions taking place [1]. Therefore, measuring the heat production of living material can provide important insights into its metabolic behavior. The quantification of the heat production rate

of isolated cells, tissue samples, whole organs, or whole organisms is the subject of what is known as biocalorimetry. In accordance with the usual conventions, the determination of the enthalpy of biomolecular interactions, such as protein–ligand-binding [2] or antigen–antibody coupling [3], is also included in the broad field of biocalorimetry. When calorimetry is applied in the frame of biological investigations, the quantities “heat” and “heat production rate” are often used as analytical parameters among others to quantify cell numbers and their change dependent on time. The determination of cell numbers has practical implications for the analysis of bacterial contaminations in body liquids [4, 5], the evaluation of the inhibitory efficacy of antibiotic drugs [6], and the monitoring of growth rates, e.g., for bioreactor control [7, 8]. Because heat production is coupled to metabolic flux, changes in the metabolism, initiated by specific inhibitory or stimulatory compounds (metabolic switches), can be analyzed in real-time [9, 10]. As an analytical tool, calorimetry mainly competes with respirometry (indirect calorimetry) which utilizes different technologies to monitor O₂ consumption and/or CO₂ production and applies caloric equivalents to determine heat production. Calorimetry, however, directly quantitates the heat production rate and other than respirometry monitors both, anaerobic and aerobic heat

✉ Johannes Lerchner
Johannes.lerchner@extern.tu-freiberg.de

¹ Institute of Physical Chemistry, TU Bergakademie Freiberg, Leipziger Str. 29, 09599 Freiberg, Germany

² Department of Animal Morphology and Physiology, School of Agricultural and Veterinary Sciences, Sao Paulo State University, Jaboticabal, SP 14884900, Brazil

³ Department of Biotechnology, Sao Paulo State University, Jaboticabal, SP 14884900, Brazil

⁴ Chair for Molecular Nutritional Medicine, TUM School of Life Science Weihenstephan, Technical University of Munich, 85354 Freising, Germany

⁵ Else Kröner-Fresenius Center for Nutritional Medicine, Technical University of Munich, Munich, Germany

production. For research addressing the thermogenic activity and underlying mechanisms of tissues and animals, heat or heat production rate represents the primary readout and is not an auxiliary parameter as in most other biological applications of calorimetry.

Calorimetry qualifies as the gold standard for studies aiming to elucidate the responsible biochemical mechanisms and signaling pathways for the recruitment of thermogenic capacity. But practical application of this technology encounters several challenges, also including the lack of suitable equipment available off the shelf. In the present work, we aim to describe a calorimeter specifically suited for measurements on small samples of thermogenic tissues. A wide variety of calorimeters are available to measure heat production in bacterial and other cell suspensions. These range from macro-calorimeters in the form of heat-balanced bioreactors [8] to classical isothermal microcalorimeters (IMCs), to miniaturized calorimeters constructed on the basis of silicon chips for measurements in the nano- and picoliter range (chip calorimeters) [11]. In contrast with that, the experimental options for an easy calorimetric analysis of aggregated samples such as small living animals or compact tissue pieces are limited. With the calorimeters available so far, samples have to be placed discontinuously in the measurement chamber, which leads to a time-consuming measurement preparation mainly caused by the time needed for temperature equilibration. As a result, the sample material may lose activity due to oxygen depletion if it is not continuously perfused with incubation medium. Typically, measurements on tissue samples are performed with commercially available IMCs, such as the multi-channel calorimeter calScreener from SymCel (Stockholm, Sweden) [12, 13] or, in the past, the well-known 2277 Thermal Activity Monitor (ThermoMetric AB, Järfälla, Sweden) [14, 15]. Especially for tissue samples and organs with high metabolic activity, specific sample preparation is required to ensure aerobicity throughout the sample volume [16, 17].

With the calorimeter presented here, it is possible to continuously transport and measure aggregated sample materials such as small pieces of tissue obtained by biopsy, but also small multicellular organisms, e.g., fly larvae. This allows automated calorimetric investigations on such biological samples. First attempts to realize an automated transport of tissue samples through the measuring channel of a chip calorimeter were made by us using the segmented flow technique [18–20]. In this technique, samples are moved because of the interface tension between an aqueous medium segment containing the sample and a water-immiscible carrier liquid. To work with a wider variety of sample materials and to increase the reliability of sample transport and positioning, we have combined a fluidic and a mechanical transport.

We here showcase the utility of our newly developed calorimeter for quantitation of heat production rates in small

organisms and high metabolic rate tissues in the fruit fly *Drosophila melanogaster*, the skeletal muscle of the tegu lizards, and the brown adipose tissue of the mouse:

Measurements on larvae of different stages and at different temperatures demonstrated how to quantify the heat production rate of highly mobile small animals. They were performed as part of a research project to study the effect of alternative oxidase (AOX) in the mitochondrial respiratory chain (RC) on thermogenesis in animals. In an alternative respiratory chain (aRC), Gibbs energy is less conserved by charge separation across the inner mitochondrial membrane. Instead, the energy is dissipated as heat [27].

We also showed that calorimetry is a valuable tool for analyzing specific heat sources in muscle cells. Due to the miniaturized measurement technique, tissue samples obtained by biopsy can be measured. The identification and quantification of the different heat sources in tegu muscles is necessary to understand the facultative endothermy during the reproductive phase of tegu [21]. Here, we used calorimetry to investigate the contribution of ANT-dependent uncoupling ([22]) to total heat production in tegu skeletal muscle tissue.

With measurements on mouse interscapular brown adipose tissue, we addressed the methodological aspects relevant for calorimetric measurements on highly metabolically active biological material. For this application, the experimental challenge is to ensure a sufficiently high oxygen supply in the given miniaturized calorimeter. Brown adipocytes are the main source of non-shivering thermogenesis in mammals. They generate heat by uncoupling the mitochondrial electron transport system from ATP synthesis.

Heat production in brown adipose tissue has already been quantified by calorimetry in the past [16, 23]. However, calorimetry holds great promise for addressing emerging research questions. These include quantifying the rate of heat production by uncoupling protein 1 (UCP1)-independent thermogenic mechanisms not only in brown adipose tissue but also in brown-like brite (brown in white) adipocytes that are recruited in white adipose tissue depots. This is relevant for preclinical research in obesity, diabetes, and cancer cachexia models, but also has translational implications ([24, 25]).

Materials and methods

Chip calorimetry

Basic technology

The chip calorimeter described here is a modified version of the calorimeters we have been using for biological investigations for several years [18, 20, 26]. Its basic technology

is characterized by the use of a silicon chip with four independently readable thermopiles (TP1 ... TP4), surrounded by two nested thermostats, which serves as a heat power detector. An essential feature is a linear, thin-walled Teflon flow channel (i.d. 1.8 mm) with a uniform cross-section along the entire length to avoid clogging of the sample material (Fig. 1A). Inside the calorimetric detector, the channel is enclosed by a PMMA mold that forms the measurement chamber, which is tightly attached to a thermopile chip. Up to two samples are introduced into the flow channel as 12- μ L segments containing the samples embedded in aqueous culture medium. In addition, a reference segment containing inert material is required to define a reference signal. In contrast with the new mechanical transport technology, in the previous versions, the segments were transported to the calorimetric detector only by a water-immiscible carrier liquid (perfluoromethyldecaline, F2 Chemicals, Preston, UK). When a sample arrives at the measurement position, it is detected by a light barrier, and the flow is stopped for heat measurement. For periodic measurement of the same samples, the segments can be moved back and forth in the flow channel by repeatedly reversing the carrier flow.

Mechanical-driven sample transport and positioning

The interface tension between the aqueous medium segment and the carrier liquid provides the force to move aggregated

sample material such as beads covered with microorganisms, soil and ore particles, and, depending on their consistency, pieces of biological tissue. To work with a wider variety of sample materials and to increase the reliability of sample transport, we have implemented a new technique for sample transport and positioning. In this new version of the calorimeter, the samples (maximum two) are transported by a polymer fiber. The fiber has knots between which the sample material is held (Fig. 1B). To move the sample segments in a defined manner, an iron anchor is attached to one end of the fiber, which is magnetically coupled to a homemade linear stepping motor drive. A mass attached to the other end of the fiber provides the counterforce to move the samples backwards (not shown). The mechanical transport can be synchronized with a fluidic transport. This means that the fixed samples and the surrounding medium are moved simultaneously at the same speed. For treatment purposes, the medium inside a segment can be replaced by any other medium containing, for example, a compound to stimulate or inhibit metabolic activity during the experiment. To do this, the sample segment is placed in the treatment port (Fig. 1A) so that the old medium can be replaced with new medium using syringe 1 (Fig. 1C). By positioning the segment at syringe 2, the displaced (old) medium is removed by syringe 2. However, this technique should only be used when a rapid treatment effect is expected. Otherwise, external treatment is required.

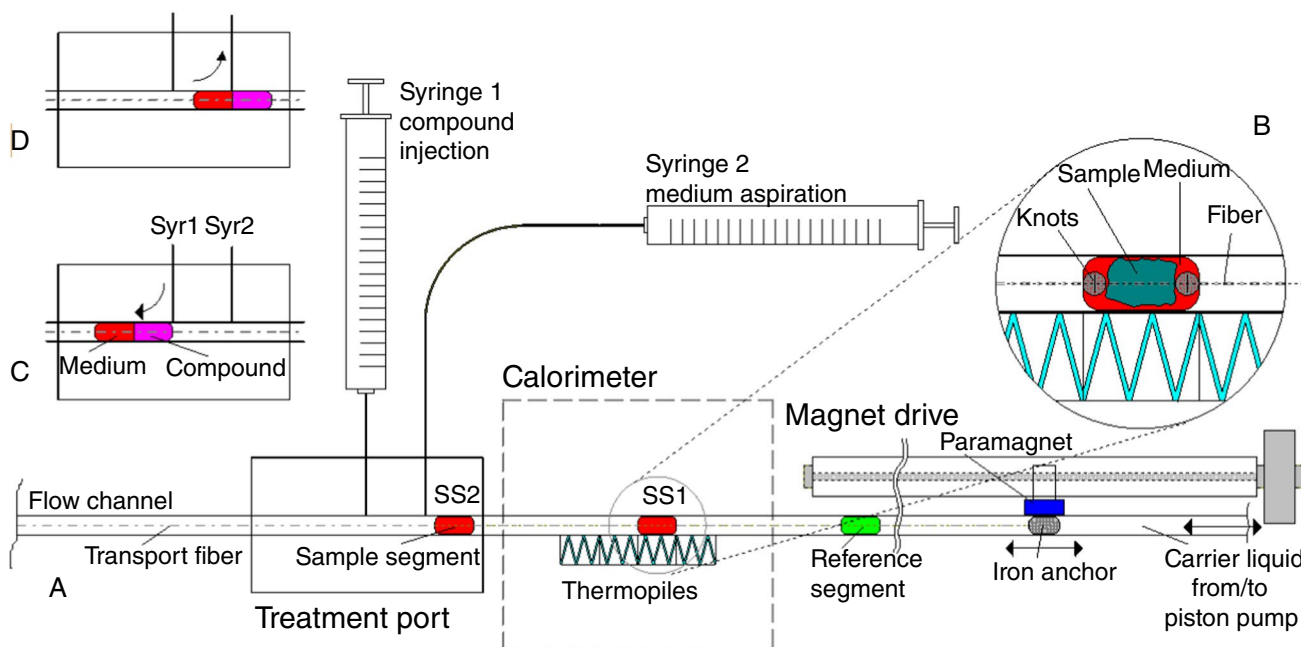


Fig. 1 Schematic representation of the calorimetric device. **A** Calorimeter with thermopile chip inside, the 1.8-mm flow channel, the transport fiber with fixed reference segment and two sample segments (one at the measurement position), the treatment port and the magnet drive. **B** An aggregated sample is held between two knots and

surrounded by aqueous medium (red). **C** To change the medium of a segment, the new medium (magenta) is injected using syringe 1 (Syr1), displacing the old one (red). **D** Excess medium is removed by syringe 2 (Syr2)

In the case that simple knots were not sufficient to hold the sample material reliably (Fig. 2A), special holders were designed. When measurements were made on fast-moving L3 instar larvae, special seals were applied to prevent them from escaping the sample segment (Fig. 2B and C). It is well known that measuring highly active material such as brown adipose tissue is quite challenging. The high oxygen consumption rate of such material requires a high surface-to-volume ratio to avoid the formation of anaerobic cores inside the sample [15, 27]. For measurements on soleus muscles of young rats and BAT of adult rats, Chinot et al. [16] implemented a rigid frame of stainless steel threads in the measurement chamber to string thread-like sample fragments approximately 20 mm long and 1 mm thick with a mass of 10–25 mg, which prevented the sample from furling. However, such a preparation is challenging to implement in a miniaturized calorimeter. To ensure short internal diffusion lengths, in this work, thread-like tissue fragments were strung along the transport fiber using attached stainless steel loops (Fig. 2D–F).

Measurements on *Drosophila* larvae

Drosophila strains and cultures

The *Drosophila* strain w^{1118} was used as control, and the AOX-expressing strain $3xtubAOX$, which carries three copies of the *C. intestinalis* AOX cDNA under control of the constitutive α -tubulin gene (*Drosophila* $\alpha Tub84B$) promoter, was used as experimental. The flies were cultured in vials containing approximately 6 mL of standard food as described [28]. In each vial, 20 female flies and 10 males were left for 12 h at 25 °C for mating and egg laying. After this period, the adult flies were discarded, and the embryos were allowed to grow until they reached the wandering third-instar larval stage (L3) or pre-pupae stage at either 25 °C or

12 °C, under a 12-h light/dark cycle. The individuals were randomly collected, briefly washed in distilled water, and dried in delicate task wipes for 10 s before weighing.

Conduction of calorimetric measurements

Calorimetric measurements were performed in *stationary medium mode* using two segments for parallel measurements of two samples. The two segments contained two individual larvae each surrounded by 8 μ L of phosphate buffer solution. Fixation of larvae in the L3-stage was challenging. Because of their high mobility, fibers with two cylindrical sponge seals in each segment were used to prevent the larvae from escaping. The reference segment also consisted of pieces of sponge material surrounded by buffer solution. The heat production of wild-type individuals in the pre-pupa and L3-stages was measured at 13 °C and 25 °C, respectively, in order to demonstrate the possible temperature working range of the calorimeter which could be relevant for the investigation of cold resistance effects. In general, three cycles with a cycle time of approximately 20 min were performed in each measurement.

Measurements on tegu lizard muscle tissue

Sample preparation

Tegu lizards were anesthetized using 5% isoflurane mixed with 100% oxygen through a facemask in an open circuit. Once the withdrawal reflex was no longer present, an endotracheal tube was inserted, and isoflurane at approximately 1% volume was administered at a rate of 0.5 mL min⁻¹ using a VetCase machine (Brasmed, São Paulo, Brazil). A surgical incision of 2 cm was made on the foreleg, and a skeletal muscle sample of approximately 40 mg was collected. The surgical procedure was

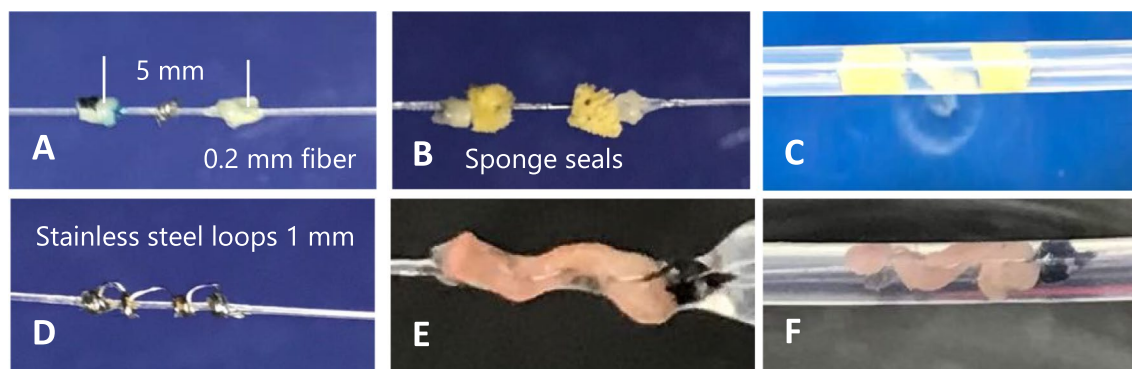


Fig. 2 Sample mounting. **A** Knots to hold samples in place. **B** Additional sponge seals for measurements on larvae. **C** Captured moving L3 instar larvae of *Drosophila*. **D** Stainless steel loops to fix filamentous

tissue fragments. **E**, **F**: A 1 mm \times 7 mm fixed BAT sample strung along the fiber

conducted under sterile conditions, and animals received intramuscular injections of meloxicam (0.2 mg kg^{-1}) for analgesia and the antibiotic agent enrofloxacin (5 mg kg^{-1}), following recommended dosages for tegus [29]. The permeabilization of muscle fibers was adapted from [30]. Briefly, the muscle samples were promptly immersed in BIOPS buffer ($2.77 \text{ mM CaK}_2\text{EGTA}$, $7.23 \text{ mM K}_2\text{EGTA}$, 20 mM imidazole , $0.5 \text{ mM dithiothreitol}$, 20 mM taurine , 50 mM K-MES , 6.56 mM MgCl_2 , 5.7 mM ATP , and $14.3 \text{ mM phosphocreatine}$; pH 7.1) kept on ice. Subsequently, the fibers were gently separated with tweezers under a magnifying glass. The samples were divided in two parts and were incubated in BIOPS buffer containing saponin ($50 \text{ }\mu\text{g mL}^{-1}$) for 30 min for chemical permeabilization of the fibers. Afterward, the tissue was transferred to 2 mL of modify MiR05 solution ($3\text{-mM MgCl}_2\cdot 6\text{H}_2\text{O}$, 20 mM taurine , $10 \text{ mM KH}_2\text{PO}_4$, 20 mM HEPES , $60 \text{ mM potassium lactobionate}$, and 110 mM sucrose ; pH 7.1) maintained at $30 \text{ }^\circ\text{C}$, without BSA and EGTA, to avoid the fatty acids quelation and to balance the amount of free calcium within the treatment solutions. This process was repeated three additional times of 10-min incubation period each one. Substrates for cell metabolism (10 mM pyruvate , 5 mM malate , 1.6 M glutamate , 1 M succinate , 0.1 mM ATP , and 20 mg L^{-1} phenol) and inhibitors of $\text{Na}^+/\text{K}^+\text{ATPase}$ (0.12 mM ouabain) and ATP synthase (oligomycin $1 \text{ }\mu\text{g mL}^{-1}$) were added to the last MiR05 incubation for the basal solution to the calorimetric measurements. For inhibiting the adenine nucleotide translocase (ANT) uncoupling contribution for heat production, carboxyatractylate (CAT, 2.4 M) was added to the basal solution.

Conduction of calorimetric measurements

Calorimetric measurements were performed in *stationary medium mode* using two segments for parallel measurements of two samples. The two segments contained tissue pieces of approximately 3 mg each surrounded by $8 \text{ }\mu\text{L}$ of medium. The sample mass was determined after the measurements. The reference segment consisted of pieces of sponge material surrounded by deionized water. After four measurement cycles, the cycling was stopped, and one of the tissues (Segment 2) was removed from the channel and treated in $500 \text{ }\mu\text{L}$ of CAT solution for 5 min. The tissue was then reinserted into the measurement channel, now surrounded by CAT solution, and the measurement continued for at least four more cycles. The tissue in Segment 1 served as control sample to exclude any faults that may occur due to the removal and re-introduction of Segment 2. Measurements were performed at $25 \text{ }^\circ\text{C}$. The measurement cycle time was approximately 20 min.

Measurements on brown adipose tissue (BAT) of mice

Animals

Mice used for tissue dissection were bred and raised in a specific pathogen-free (SPF) mouse facility at the Animal Research Center (ARC, Technical University of Munich), registered at the veterinary office of the local district government in Freising, Germany (Az. 32–568). All procedures were conducted in compliance with the German Animal Welfare Act by trained personnel. Mice are group housed under controlled climate conditions in individually ventilated cages adjusted to 55% relative humidity at room temperature ($23 \text{ }^\circ\text{C}$). They were kept in a 12/12-h light–dark cycle with ad libitum access to water and regular chow (fortified complete feed for breeding mice from ssniff Spezialdiäten GmbH, Soest, Germany; metabolizable energy 14 MJ/kg , #V1124-300). All mice used in this study are derived from inbred strains (C57BL/6 J/N or 129S6sv/sv Tac).

Tissue collection and preparation

Interscapular brown adipose tissue was sampled from adult mice at the age of 6–11 weeks. Mice were euthanized by exposure to CO_2 . For dissection, the body was positioned in prone orientation, and the fur soaked with 70% ethanol. An incision was made between the shoulder blades and expanded to reveal the brown adipose tissue depot beneath the skin. The depot was blotted on Whatman paper and separated from adhering white adipose tissue and muscle fibers. The excised tissue was covered with buffer to prevent desiccation. Using a sharp scalpel and magnifying glasses, the tissue was then sliced into slender strips which were threaded through the loops of the sample holder (Fig. 2D and E).

Conduction of calorimetric measurements

Calorimetric measurements were performed in both *stationary medium mode* and *continuous flow mode*. In *stationary medium mode*, two segments were used for parallel measurements of two samples. The two segments contained compact pieces of BAT of $0.3\text{--}3 \text{ mg}$ surrounded by up to $10 \text{ }\mu\text{L}$ of medium A (DMEM XF pH 7.4, 25 mM glucose , 1 mM pyruvate , and 2 mM glutamate). This medium is usually used in experiments with isolated adipocytes. To avoid loss of tissue, small pieces of inert sponge material were added. The reference segment also consisted of pieces of sponge material surrounded by buffer solution. In general, three cycles with a cycle time of approximately 20 min were performed for each measurement. Due to heat production rate drift, only the heat production rate value of the first cycle was used. In the *continuous flow mode*, only one piece of BAT

was placed in the calorimeter and continuously perfused with the medium. The sample mass varied between 0.5 and 3.5 mg. It was determined immediately after each measurement. To be consistent with the measurement conditions described in [16], we also performed measurements with Medium B (: Krebs–Ringer buffer: pH 7.3, 11 mM glucose, 1.2 mM Mg Cl₂·6H₂O, 2.5 mM Ca Cl₂·2H₂O, 1.2 mM Na H₂ PO₄, 20 mM NaHCO₃, 117 mM NaCl, and 4.7 mM KCl). Changing from medium A to medium B had no effect on the heat production rate (not shown here). Therefore, we used Medium B for all further measurements. In a third set of measurements, samples were incubated in the medium B for 15 min prior to the measurements. The medium was continuously gassed with carbogen (95% oxygen and 5% carbon dioxide). In addition, a few indicative measurements were performed using the technique described in [10], which allows flushing of the channel jacket and a surrounding gas chamber with carbogen. All measurements were performed at 37 °C. The operating procedures and the derivation of the heat production rates from the thermopile signals are explained in the “Operation modes” section.

Results and discussion

Methodological studies

Operation modes

The calorimeter can be operated in different modes, a *stationary medium mode* and a *continuous flow mode*. With respect to the medium, the first one is a stop-flow mode. This means that the medium segments are transported synchronously with the sample pieces using the segmented flow technique, and that the medium is stationary during the measurement period. In *continuous flow mode*, the sample is held at the measurement position during the measurement period while being perfused with an appropriate medium at a constant flow rate. In this mode, no additional carrier liquid is used.

A major advantage of *stationary flow mode* is that individual sample segments with different media can be measured simultaneously (sequentially) and cyclically repeated [18]. In addition, the calibration effort is low [18], and the measurement accuracy is higher than in the medium flow mode, also because TP4, the thermopile furthest from the sample, can be used to compensate for the effect of external temperature disturbances. The stationary flow mode is not applicable when the oxygen uptake rate of the sample is limited by the oxygen diffusion rate through the measurement chamber and the flow channel wall.

A typical signal (output voltage of TP2 corrected by TP4) of a measurement cycle obtained in *stationary medium mode*

from the larvae measurements is shown in Fig. 3A and B. The reference segment and the two sample segments are successively placed at the measurement position and then measured statically. From the differences of the steady-state signals, the heat power is derived using the calorimetric sensitivity. Due to the axial heat transfer, the signal

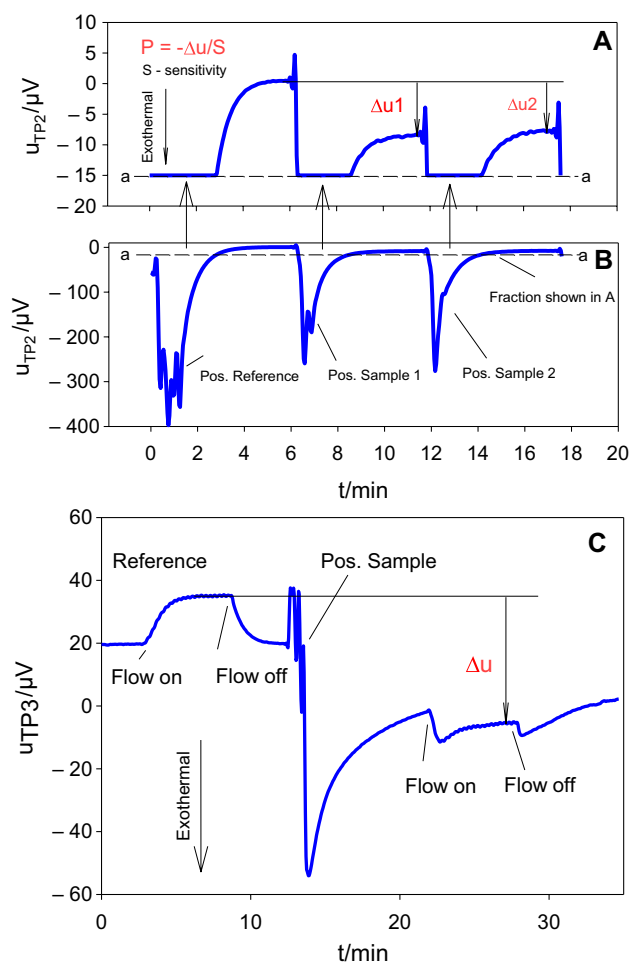


Fig. 3 Representative thermopile signals obtained in stationary medium mode (A, B) and in medium flow mode (C). A, B Signal response (TP2) for one measurement cycle in an experiment with one *Drosophila* pre-pupa in each of the two sample segments. A Fraction of the complete signal shown in B above line a-a, separately displayed for better resolution. Steady state is reached approximately 5 min after sample positioning. The heat production rates correspond to the differences Δu_1 and Δu_2 , respectively, with respect to the signal level for the reference segment. Due to incomplete temperature control of the sample during transport, the positioning of the segments is associated with strong exothermic signal peaks. C Signal response (TP3) for a measurement on a BAT sample in medium flow mode. An endothermic signal shift at constant medium flow (20 $\mu\text{L min}^{-1}$) measured for the reference is due to incomplete sample temperature control. The transient exothermic heat effect observed after sample positioning is caused by metabolic heat production. A defined heat production rate is obtained when the sample is perfused at constant medium flow (20 $\mu\text{L min}^{-1}$). Negative deflections of the thermopile voltage correspond to exothermic heat effects

contributions of the adjacent thermopiles TP6 and TP8 must be added.

Samples with high metabolic activity must be continuously perfused to ensure a sufficiently high oxygen delivery rate (*continuous flow mode*). Since the efficiency of the heat exchange between the medium flow and the thermostat is not perfect in the given instrument, a flow effect is measured in the signal, the magnitude of which depends on the flow rate and the ambient temperature. Therefore, timely reference measurements must be made at the same flow rate.

The signal shown in Fig. 3C represents a measurement on a BAT sample in which the reference flow effect was measured before the sample was placed in the measurement position. The sample was then moved to the thermopile (TP3), causing a strong exothermic deflection of the signal, the magnitude of which rapidly decreased mainly due to oxygen depletion. The oxygen depletion is then counteracted by a subsequent medium flow. The difference between the steady-state signal levels provides the heat production rate value. Sensitivity was determined experimentally by Joule heating using a cylindrical platinum wire resistor placed above TP3. The resistor was attached to a fiber and transported to the heat power detector in the same manner as the sample segments. Due to convective heat transfer in the flow direction, the samples were placed above TP3. The flow rate dependencies of the total sensitivity and the contributions of the four thermopiles are shown in Fig. 4 for a heat source at TP3. For comparison, the static sensitivity and the total sensitivity at $20 \mu\text{L min}^{-1}$ are also shown for a heat source at TP2.

Sodium sulfite tests

To clarify the oxygen supply to the measurement chamber in *stationary medium mode*, the oxidation of small samples of sodium sulfite ($10 \mu\text{L}$ of 0.6 M aqueous solution each)

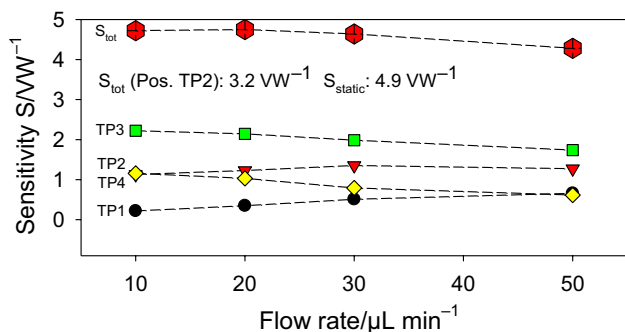


Fig. 4 Flow dependence of the calorimetric sensitivity for a heat source positioned at TP3 and a flow directed from TP4 to TP1. The total sensitivity S_{tot} is the sum of the contributions from all four thermopiles. S_{tot} (Pos. TP2) is the total sensitivity for a heat source at TP2 and a flow rate of $20 \mu\text{L min}^{-1}$. S_{static} is the sensitivity at TP2 and zero flow

was measured. Since the oxidation of sulfite to sulfate is fast [31], the oxygen consumption rate derived from the measured heat production rate using the reaction enthalpy ($\Delta H = -540 \text{ kJ mol}^{-1} \text{ O}_2$ [32]) can be assumed as the maximum oxygen supply rate. Once the oxygen dissolved in approximately $10 \mu\text{L}$ is consumed within less than 1 min, the oxygen supply is then diffusion controlled and rapidly decreases, depleting the oxygen in the measurement chamber environment (Fig. 7).

Measurements on Drosophila larvae

The heat production rate data were derived from the calorimetric signals according to Fig. 3. As shown by the measured heat production rate curves (Fig. 5A), the heat production of the larvae generally changes slightly with time. Therefore, comparisons were made using the

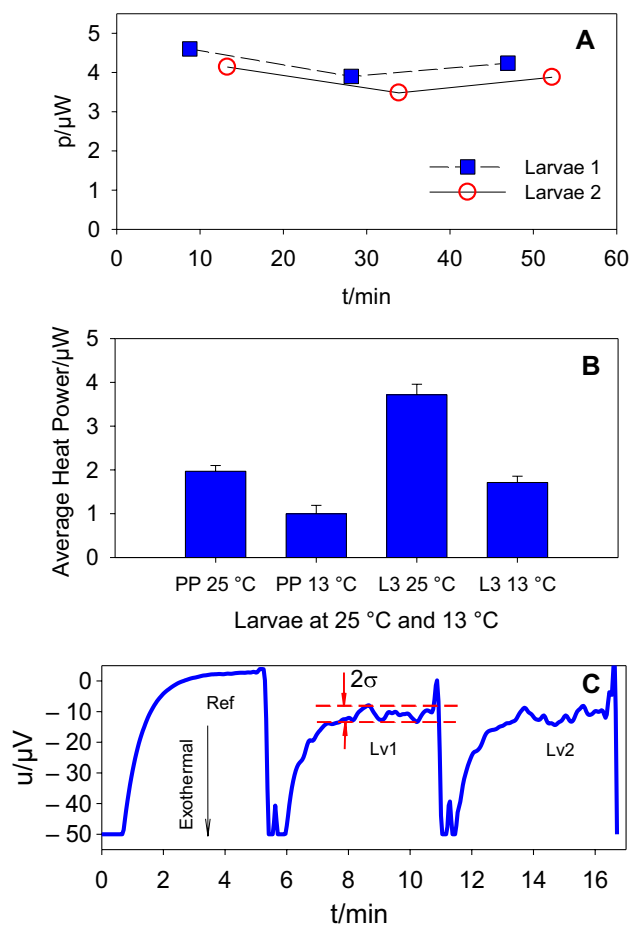


Fig. 5 Heat production rates of *Drosophila* larvae. **A** Heat production rate of two individual L3-stage larvae measured over three cycles. **B** Average heat production rates of L3 and pre-pupa (PP) individuals at $13 \text{ }^\circ\text{C}$ and $25 \text{ }^\circ\text{C}$. **C** Typical calorimetric signal from an L3-stage larva (σ —standard deviation of the noise, Ref—reference segment, and Lv1 and Lv2—two individual larvae). Negative deflections of the thermopile voltage correspond to exothermic heat effects

average of the first cycle data. As expected, the heat production rate of L3-stage larvae exceeds that of pre-pupae (Fig. 5B). This was observed at both 25 °C and 13 °C. From the heat production rates measured at both temperatures, a temperature coefficient of about $Q_{10} = 2$ is obtained for both larval species, which is in good agreement with corresponding observations for *Drosophila melanogaster* [33]. When L3-stage larvae are engaged in a segment, they move strongly (see video in Fig. S1). The motion of the engaged larvae considerably affects the characteristics of the calorimetric signal. In contrast with the smooth signals obtained from pre-pupae (Fig. 3A), highly noisy signals were observed for L3-stage larvae (Fig. 5C). The standard deviation of the noise can be used to quantify the motion intensity. There are significant differences between wild-type and AOX larvae. For the former, we found a standard deviation of $= 0.5 \pm 0.04 \mu\text{V}$, while for AOX larvae, we measured $= 0.9 \pm 0.1 \mu\text{V}$. This is in agreement with our previous publication showing more peristaltic movements and crawling by the AOX-expressing flies [34].

Measurements on tegu lizard muscle tissue

To apply calorimetry to study the contribution of ANT-dependent uncoupling ([35]) to the overall heat production in skeletal muscle tissue of tegu, pieces of muscle tissue were treated with the ANT inhibitor, CAT. The heat production rate data of a CAT treated sample and a control sample of one measurement cycle are derived as shown in Fig. 3. The variation of the heat production rate with time is shown in Fig. 6 for one measurement example. After starting the treatment with CAT, a clear inhibition effect was observed. The inhibition effect was quantified by linear regressions and extrapolations of the heat production rate curves before and after the start of treatment, as shown in Fig. 6. In general, a slight decrease in the heat production rate with time was observed, perhaps due to the change of the incubation conditions. To determine the inhibition effect StepCAT (Fig. 6), linear regressions of the heat production rate curve before and after the start of treatment were performed. StepCAT is read as the distance between the regression lines at the mean time of the last point before and the first point after the start of treatment. To account for variations in sample mass, heat production rate steps were normalized to the average heat production rate of the four cycles prior to the start of treatment. On average, inhibition reduced heat production by approximately 36%. This fraction is related to the heat production sustained by mitochondrial respiration (actions of RC complexes I-IV) and the ANT-induced leak.

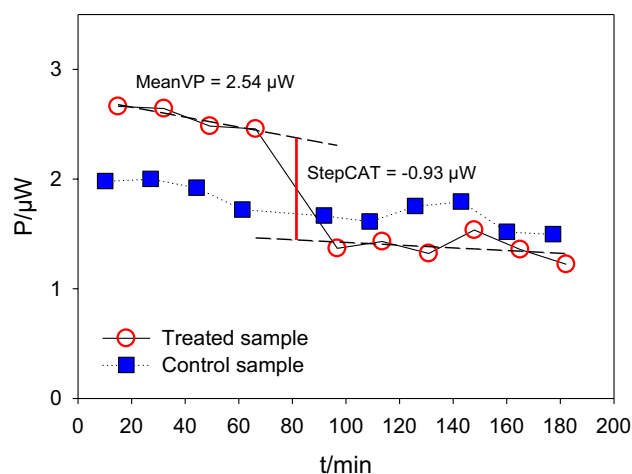


Fig. 6 Time dependence of the heat production rate of a treated and a control sample, respectively, of tegu muscle tissue. Treatment with CAT was started after the fourth cycle. MeanVP: average heat production rate of the four cycles prior to the start of treatment. StepCAT: CAT treatment effect

Measurements on brown adipose tissue (BAT) of mice

We here addressed the methodological aspects relevant to calorimetric measurements on highly metabolically active biological materials, showcased for interscapular brown adipose tissue of the mouse. For this application, the experimental challenge is to ensure a sufficiently high level of oxygen supply in the given miniaturized calorimeter. In particular, the sample must be prepared to avoid anoxic cores in the interior, as observed in different operation modes and sample preparations. To optimize these parameters, the heat production rates of BAT samples from WT mice were measured as a function of mass (Fig. 8). Measurements were performed in two modes, *stationary medium mode* and *continuous flow mode*. The results differ drastically for both operation modes. The lower heat production rates of the samples measured in the *stationary medium mode* are most likely explained by oxygen limitation. Since the treatment with antimycin A had no significant effect on the heat production rate (data not shown here), it is assumed that the measured heat production rate is not caused by mitochondrial respiration and could, therefore, be mainly determined by anaerobic metabolism. In *continuous flow mode*, oxygen is supplied by perfusion, resulting in increased heat production. However, even in *continuous flow mode*, a saturation effect can be observed above 2 mg of BAT mass.

Approximately 10 min after sample introduction, which is the time required to obtain a near steady-state signal, an oxygen delivery rate of approximately 10 pmol s^{-1} should still be available (Fig. 7). This corresponds to a heat production rate of $4.3 \mu\text{W}$ at an oxycaloric equivalent of 430 kJ mol^{-1}

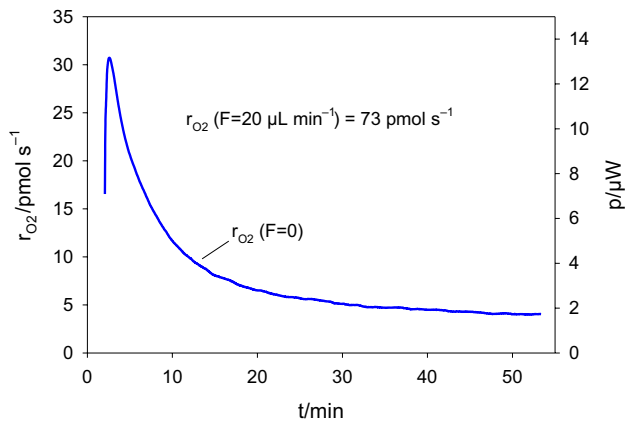


Fig. 7 Time dependence of the oxygen consumption rate r_{O_2} of 10 μL of 0.6 M sodium sulfite solution, controlled by oxygen diffusion, and the oxygen delivery rate established by a constant medium flow of $F=20 \mu\text{L min}^{-1}$ at 37°C . The curve also represents the metabolic heat production rate p (right-hand ordinate) which is equivalent to the shown oxygen consumption rate (heat equivalent of $430 \text{ kJ mol}^{-1} \text{ O}_2$)

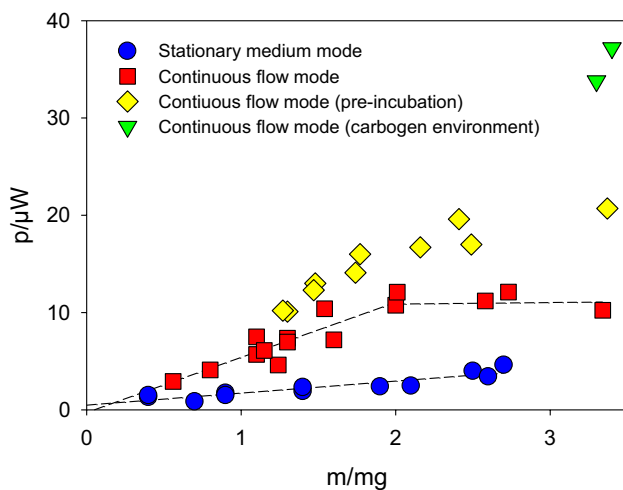


Fig. 8 Heat production of BAT samples as a function of mass, measured in *stationary medium mode* (blue circles) and in *continuous flow mode* (red squares). Data obtained for samples measured in *continuous flow mode* but pre-incubated for 15 min in medium gassed with carbogen are shown separately (yellow diamonds). Two data points (green triangles) represent heat production rate data measured in a surrounding carbogen atmosphere

O_2 [16], considerably higher than the heat production rate data measured in *stationary medium mode*. When the sample is continuously perfused with medium (*continuous flow mode*) at a flow rate of 20 mL min^{-1} , the oxygen delivery rate due to liquid flow is constant throughout the experiment at 73 pmol s^{-1} , assuming an oxygen solubility in water at 37°C of $0.218 \text{ mmol L}^{-1}$. As shown by the calorimetric data obtained in the *continuous flow mode*, a significantly increased oxygen delivery rate leads to an increased heat

production of the sample. The limitation at $11 \mu\text{W}$, corresponding to an oxygen consumption rate of 26 pmol s^{-1} , above a sample mass of 2 mg cannot be explained by the given oxygen delivery rate alone. To explain the discrepancies, limitations of oxygen diffusion into the sample with increasing sample size must be considered.

When oxygen enters the sample, it is metabolized. Therefore, it cannot penetrate the entire sample if its size exceeds a critical limit. As a result, an anaerobic core is formed, and the mass specific heat production is reduced ([15] and references therein). This so-called "crowding effect" was observed by Singer et al. [15] when they measured the heat production of rat liver tissue slices. The critical depth of tissue aerobiosis depends on the specific heat production per unit mass, the diffusion coefficient and the solubility of oxygen in the sample material, as well as the partial pressure of oxygen in the medium. Assuming a cylindrical geometry of the sample, Daut and Elzinga [27] calculated a critical partial pressure depending on the radius of the sample, which is the minimum pressure to achieve complete aerobiosis. Based on the model used, a critical radius of a cylindrical sample can be calculated for the atmospheric oxygen pressure in the medium. With a mass specific heat production of 5 mW cm^{-3} , derived from the heat production rate curve in Fig. 7, and using Daut's data for diffusion coefficient and oxygen solubility ($D=1.09 \cdot 10^5 \text{ cm}^2 \text{ s}^{-1}$, $=0.0296 \text{ mL cm}^{-3} \text{ atm}^{-1}$ for rat heart muscle tissue), a radius of $r=0.3 \text{ mm}$ results. This is close to the radius of a BAT tissue sample of 7-mm length and 2-mg mass (0.27 mm). This is a rather rough estimate because the samples are not truly cylindrical as shown in Fig. 2E and F, additional curling may occur during transport, precise data for D and are not available for BAT, and there may be local oxygen gradients in the surrounding medium. Nevertheless, it seems obvious that diffusion limitations within the sample are mainly responsible for the saturation effect in the heat production rate curve (Fig. 7). When the samples were incubated in medium prior to the calorimetric measurements, slightly increased heat production rates were observed (Fig. 8, continuous flow mode (pre-incubation)), possibly due to improved oxygen diffusion insight of the sample. In this case, a mass specific heat production rate of about $9 \mu\text{W mg}^{-1}$ was measured, which is considerably higher than the basal heat production rate measured by Girardier et al. [36] for rat BAT in both summer and winter ($5.5 \mu\text{W mg}^{-1}$ and $1.9 \mu\text{W mg}^{-1}$, respectively).

Diffusion limitation can also explain the exceptionally low values obtained in the *stationary medium mode*. In this case, the samples are very compact and have an almost spherical shape. In addition, they are in contact with the channel wall, which further restricts the access of oxygen into the sample. In conclusion, the useful mass range could be extended by more precise sample preparation to further reduce furling and by increasing the oxygen partial pressure

in the medium. As it was demonstrated previously [10], the small size of a chip calorimeter provides the opportunity to create a defined gas atmosphere around the measurement chamber quite easily. First indicative measurements have shown that using the technique described in [10], but flushing the channel jacket and the surrounding gas chamber with carbogen, no saturation effects could be observed at least up to 3-mg BAT mass (Fig. 8).

Conclusions

Calorimetry is a useful tool to quantify non-specifically the overall intensity of metabolic processes in living matter. The method is particularly interesting if the sources of thermogenesis in bodies have to be analyzed. If investigations have to be performed at the tissue level or in case of the study of the heat production in small animals, direct calorimetry is the preferred method in comparison with indirect calorimetry, because the directly measured heat includes anaerobic contributions.

An efficient sample handling technique is a prerequisite for the practical application of direct calorimetry for measurements on tissue samples or small animals if a sufficiently high throughput is to be achieved. A new sample transport system adapted to a highly sensitive chip calorimeter meets the requirements for routine use of the method in a biomedical laboratory.

The degree of miniaturization of the device, resulting from the use of thin-film silicon thermopile heat power detectors, allows measurements to be made on small samples in the lower milligram range and below, which, in turn, simplifies the design of the transport facilities. Sample miniaturization is of practical interest, for example, when biopsy tissue samples need to be measured. It has been shown again [20], that the small thermal time constants of chip calorimeters, which are a consequence of the small sample size, allow the quantification of the motion intensity of living samples.

By the standards of modern biomedical and biochemical analysis, the calorimeter described here does not represent high-throughput technology, nor are the sample volumes used spectacularly small. High-throughput technology is generally defined as a sample throughput of > 10,000 samples per day [37]. And today, microfluidic technology also allows the generation of sample droplets down to the picoliter range [38]. However, compared to state-of-the-art microcalorimeters, and especially compared to their ability to measure aggregated samples such as tissue pieces (e.g., calScreener from SymCel), the reduction of the measurement duration or measurement cycle time to approximately 10 min represents a significant advance. This is made possible not only by the newly developed sample transport

technology. Sample sizes in the microliter and submicroliter range are another prerequisite.

The instrument is suitable for testing a wide variety of sample materials. Heat production of live *Drosophila* larvae, biopsied tegu lizard muscle, and metabolically active brown adipose tissue have been successfully measured. Treatment with biochemical inhibitors allows the analysis of specific heat sources in muscle cells as demonstrated with tegu lizard tissue. The contribution of ANT-driven uncoupling in mitochondria to the decoupled (i.e., with suppressed OXPHOS) heat production in muscle cells was quantified. Similarly, the contribution of SERCA-catalyzed Ca^{2+} -futile cycling, another important source of heat in muscle cells, could be determined. This would open the possibility to study the seasonal dependence of these thermogenic effects in tegu lizards. The measurements on *Drosophila* L3 larvae demonstrated the potential of high dynamic chip calorimetry to elucidate short-term thermal effects, such as those caused by movement. The potential for measurements below room temperature may be of interest when investigating cold resistance effects, for example, in genetically modified species [39].

Measurements on BAT samples have shown that biological tissues with extremely high metabolic activity can be measured if sufficient oxygen is supplied to the samples. This can be achieved by providing a large sample surface and short diffusion paths in the sample by using a special sample holder, operating the calorimeter in flow-through mode, and completely flushing the surroundings of the measuring chamber and the sample channel with oxygen. Under these conditions, the calorimeter presented here may also be of interest for the investigation of other highly active tissues, such as the flight muscles of various insects [40].

Supplementary Information The online version contains supplementary material available at <https://doi.org/10.1007/s10973-024-13183-8>.

Acknowledgements This study was supported by FAPESP grant 2021/10910-0 and CAPES PrInt (Finance Code 001, Process: 88887.194785/2018-00) to KCB&JL, by FAPESP grant 2021/06711-2 and CNPq grants 424562/2018-9 and 308940/2021-0 to MTO; CNPq grant 141001/2019-4 to GSG, as well as by DFG transregio collaborative research center “BATenergy” (TRR333/1; project# 450149205) and Else Kröner Fresenius Stiftung (2017_A108 e EKFZ) to MK. Capes and FAPESP payed two trips by JL. JL is grateful to Michael Piller (Freiberg) for assistance in device development. We thank the doctoral candidates Anna Schwaiger, Josef Oeckl, Johanna Bruder, Akim Strohmeyer, and Hildigunnur Hermannsdottir for hands-on assistance and the TUM Animal Research Center (ARC) for infrastructural support.

Author contributions All authors contributed to the study conception and design. Material preparation, data collection, and analysis were performed by MH, LSH, GSG, and JL. The first draft of the manuscript was written by LSH, GSG, and JL, and all authors commented on the previous versions of the manuscript. All authors read and approved the final manuscript.

Funding Open Access funding enabled and organized by Projekt DEAL.

Data availability The datasets used and/or analyzed during the current study are available from the corresponding author upon reasonable request.

Declarations

Conflict of interest The authors declare that the research was conducted in the absence of any commercial or financial relationships that could be construed as a potential conflict of interest.

Ethical approval Not applicable.

Consent to participate Not applicable.

Consent for publication Not applicable.

Open Access This article is licensed under a Creative Commons Attribution 4.0 International License, which permits use, sharing, adaptation, distribution and reproduction in any medium or format, as long as you give appropriate credit to the original author(s) and the source, provide a link to the Creative Commons licence, and indicate if changes were made. The images or other third party material in this article are included in the article's Creative Commons licence, unless indicated otherwise in a credit line to the material. If material is not included in the article's Creative Commons licence and your intended use is not permitted by statutory regulation or exceeds the permitted use, you will need to obtain permission directly from the copyright holder. To view a copy of this licence, visit <http://creativecommons.org/licenses/by/4.0/>.

References

- Diederichs F. Principles of heat production in skeletal muscle cells. *Mol Biophys Biochem.* 2017;2:1–14.
- Paketyrytė V, Zubrienė A, Ladbury JE, et al. Intrinsic thermodynamics of protein-ligand binding by isothermal titration calorimetry as aid to drug design. *Methods Mol Biol.* 2019;1964:61–74. https://doi.org/10.1007/978-1-4939-9179-2_5.
- Frasca V. Biophysical characterization of antibodies with isothermal titration calorimetry. *J Appl Bioanal.* 2016;2:90–102. <https://doi.org/10.17145/jab.16.013>.
- Tschudin-Sutter S, Braissant O, Erb S, et al. Growth patterns of *Clostridium difficile*: correlations with strains, binary toxin and disease severity: a prospective cohort study. *PLoS ONE.* 2016;11:e0161711. <https://doi.org/10.1371/journal.pone.0161711>.
- Braissant O, Theron G, Friedrich SO, et al. Comparison of isothermal microcalorimetry and BACTEC MGIT960 for the detection of the metabolic activity of *Mycobacterium tuberculosis* in sputum samples. *J Appl Microbiol.* 2020;128:1497–502. <https://doi.org/10.1111/jam.14549>.
- Tellapragada C, Hasan B, Antonelli A, et al. Isothermal microcalorimetry minimal inhibitory concentration testing in extensively drug resistant Gram-negative bacilli: a multicentre study. *Clin Microbiol Infect.* 2020;26:1413.e1–1413.e7. <https://doi.org/10.1016/j.cmi.2020.01.026>.
- Türker M. Development of biocalorimetry as a technique for process monitoring and control in technical scale fermentations. *Thermochim Acta.* 2004;419:73–81. <https://doi.org/10.1016/j.tca.2004.01.036>.
- von Stockar U, Marison IW. Large-scale calorimetry and biotechnology. *Thermochim Acta.* 1991;193:215–42. [https://doi.org/10.1016/0040-6031\(91\)80185-L](https://doi.org/10.1016/0040-6031(91)80185-L).
- Dejean L, Beauvoit B, Bunoust O, et al. The calorimetric-respirometric ratio is an on-line marker of enthalpy efficiency of yeast cells growing on a non-fermentable carbon source. *Biochim Biophys Acta.* 2001;1503:329–40. [https://doi.org/10.1016/S0005-2728\(00\)00210-3](https://doi.org/10.1016/S0005-2728(00)00210-3).
- Lerchner J, Sartori MR, Volpe POL, et al. Direct determination of anaerobe contributions to the energy metabolism of *Trypanosoma cruzi* by chip calorimetry. *Anal Bioanal Chem.* 2019;411:3763–8. <https://doi.org/10.1007/s00216-019-01882-3>.
- Wang S, Sha X, Yu S, et al. Nanocalorimeters for biomolecular analysis and cell metabolism monitoring. *Biomicrofluidics.* 2020;14:11503. <https://doi.org/10.1063/1.5134870>.
- Braissant O, Keiser J, Meister I, et al. Isothermal microcalorimetry accurately detects bacteria, tumorous microtissues, and parasitic worms in a label-free well-plate assay. *Biotechnol J.* 2015;10:460–8. <https://doi.org/10.1002/biot.201400494>.
- Gros SJ, Holland-Cunz SG, Supuran CT, et al. Personalized treatment response assessment for rare childhood tumors using microcalorimetry-exemplified by use of carbonic anhydrase IX and aquaporin 1 inhibitors. *Int J Mol Sci.* 2019. <https://doi.org/10.3390/ijms20204984>.
- Bach F, Singer D, Bauer M, et al. Prediction of recovery after ischemia: a microcalorimetric and biochemical study of rat liver tissue. *Thermochim Acta.* 1995;251:161–72. [https://doi.org/10.1016/0040-6031\(94\)02042-M](https://doi.org/10.1016/0040-6031(94)02042-M).
- Singer D, Schunck O, Bach F, et al. Size effects on metabolic rate in cell, tissue, and body calorimetry. *Thermochim Acta.* 1995;251:227–40. [https://doi.org/10.1016/0040-6031\(94\)02072-V](https://doi.org/10.1016/0040-6031(94)02072-V).
- Chinet A, Clausen T, Girardier L. Microcalorimetric determination of energy expenditure due to active sodium-potassium transport in the soleus muscle and brown adipose tissue of the rat. *J Physiol.* 1977;265:43–61. <https://doi.org/10.1113/jphysiol.1977.sp011704>.
- Daut J, Elzinga G. Heat production of quiescent ventricular trabeculae isolated from guinea-pig heart. *J Physiol.* 1988;398:259–75. <https://doi.org/10.1113/jphysiol.1988.sp017041>.
- Hartmann T, Barros N, Wolf A, et al. Thermopile chip based calorimeter for the study of aggregated biological samples in segmented flow. *Sens Actuators, B Chem.* 2014;201:460–8. <https://doi.org/10.1016/j.snb.2014.05.024>.
- Wolf A, Hartmann T, Bertolini M, et al. Toward high-throughput chip calorimetry by use of segmented-flow technology. *Thermochim Acta.* 2015;603:172–83. <https://doi.org/10.1016/j.tca.2014.10.021>.
- Lerchner J, David KA, Unger FT, et al. Continuous monitoring of drug effects on complex biological samples by segmented flow chip calorimetry. *J Therm Anal Calorim.* 2017;127:1307–17. <https://doi.org/10.1007/s10973-016-6081-7>.
- Tattersall GJ, Leite CAC, Sanders CE, et al. Seasonal reproductive endothermy in tegu lizards. *Sci Adv.* 2016;2: e1500951. <https://doi.org/10.1126/sciadv.1500951>.
- Mak IT, Shrago E, Elson CE. Modification of liver mitochondrial lipids and of adenine nucleotide translocase and oxidative phosphorylation by cold adaptation. *Biochim Biophys Acta.* 1983;722:302–9. [https://doi.org/10.1016/0005-2728\(83\)90077-4](https://doi.org/10.1016/0005-2728(83)90077-4).
- Janský L, Musacchia XJ. Regulation of depressed metabolism and thermogenesis. 1976.
- Petruzzelli M, Schweiger M, Schreiber R, et al. A switch from white to brown fat increases energy expenditure in cancer-associated cachexia. *Cell Metab.* 2014;20:433–47. <https://doi.org/10.1016/j.cmet.2014.06.011>.

25. Becher T, Palanisamy S, Kramer DJ, et al. Brown adipose tissue is associated with cardiometabolic health. *Nat Med*. 2021;27:58–65. <https://doi.org/10.1038/s41591-020-1126-7>.
26. Lerchner J, Volpe POL, Lanaro C, et al. A chip calorimetry-based method for the real-time investigation of metabolic activity changes in human erythrocytes caused by cell sickling. *J Therm Anal Calorim*. 2019;136:771–81. <https://doi.org/10.1007/s10973-018-7692-y>.
27. Daut J, Elzinga G. Substrate dependence of energy metabolism in isolated guinea-pig cardiac muscle: a microcalorimetric study. *J Physiol*. 1989;413:379–97. <https://doi.org/10.1113/jphysiol.1989.sp017659>.
28. Fernandez-Ayala DJM, Sanz A, Vartiainen S, et al. Expression of the *Ciona intestinalis* alternative oxidase (AOX) in *Drosophila* complements defects in mitochondrial oxidative phosphorylation. *Cell Metab*. 2009;9:449–60. <https://doi.org/10.1016/j.cmet.2009.03.004>.
29. Zena LA, Dillon D, Hunt KE, et al. Hormonal correlates of the annual cycle of activity and body temperature in the South-American tegu lizard (*Salvator merianae*). *Gen Comp Endocrinol*. 2020;285: 113295. <https://doi.org/10.1016/j.ygcen.2019.113295>.
30. Hughey CC, Hittel DS, Johnsen VL, et al. Respirometric oxidative phosphorylation assessment in saponin-permeabilized cardiac fibers. *J Vis Exp*. 2011. <https://doi.org/10.3791/2431>.
31. Ogawa S, Shimizu Y, Tone S, et al. Kinetics of the oxidation of aqueous sodium sulfite solutions with air. *J Chem Eng Japan / JCEJ*. 1982;15:400–2. <https://doi.org/10.1252/jcej.15.400>.
32. Roine A (2011) HSC Chemistry 7.1. Software for process simulation, reactions equations, heat and material balances, equilibrium calculations, electrochemical cell equilibriums, Eh-pH Diagrams—Pourbaix diagram, Pori (Finland)
33. Kuntz SG, Eisen MB. *Drosophila* embryogenesis scales uniformly across temperature in developmentally diverse species. *PLoS Genet*. 2014;10: e1004293. <https://doi.org/10.1371/journal.pgen.1004293>.
34. Garcia GS, Othonicar MF, Oliveira MT, et al. An affordable and efficient “homemade” platform for *Drosophila* behavioral studies, and an accompanying protocol for larval mitochondrial respirometry. *J Vis Exp*. 2021. <https://doi.org/10.3791/62669>.
35. Brenner C, Subramaniam K, Pertuiset C, et al. Adenine nucleotide translocase family: four isoforms for apoptosis modulation in cancer. *Oncogene*. 2011;30:883–95. <https://doi.org/10.1038/onc.2010.501>.
36. Girardier L. Catecholamine binding and modulation of the thermogenic effect in brown adipose tissue of the rat. In: Jansky, L. & Musacchia, X. J. (ed.) *Regulation of Depressed Metabolism*. pp 196–212, 1976
37. Mayr LM, Bojanic D. Novel trends in high-throughput screening. *Curr Opin Pharmacol*. 2009;9:580–8. <https://doi.org/10.1016/j.coph.2009.08.004>.
38. Saupé M, Wiedemeier S, Gastrock G, et al. Flexible toolbox of high-precision microfluidic modules for versatile droplet-based applications. *Micromachines*. 2024. <https://doi.org/10.3390/mi15020250>.
39. Saari S, Garcia GS, Bremer K, et al. Alternative respiratory chain enzymes: therapeutic potential and possible pitfalls. *Biochim Biophys Acta Mol Basis Dis*. 2019;1865:854–66. <https://doi.org/10.1016/j.bbadis.2018.10.012>.
40. Gaviraghi A, Correa Soares JBR, Mignaco JA, et al. Mitochondrial glycerol phosphate oxidation is modulated by adenylates through allosteric regulation of cytochrome c oxidase activity in mosquito flight muscle. *Insect Biochem Mol Biol*. 2019;114: 103226. <https://doi.org/10.1016/j.ibmb.2019.103226>.

Publisher's Note Springer Nature remains neutral with regard to jurisdictional claims in published maps and institutional affiliations.